

Kinetic Simulations of Magnetic Reconnection in Partially Ionized Plasmas

J. Jara-Almonte, H. Ji, J. Yoo, M. Yamada, and W. Fox
Princeton Plasma Physics Laboratory, Princeton, New Jersey 08543, USA

W. Daughton
Los Alamos National Laboratory, Los Alamos, New Mexico 87545, USA

 (Received 31 August 2018; published 9 January 2019)

Fast magnetic reconnection occurs in nearly all natural and laboratory plasmas and rapidly releases stored magnetic energy. Although commonly studied in fully ionized plasmas, if and when fast reconnection can occur in partially ionized plasmas, such as the interstellar medium or solar chromosphere, is not well understood. This Letter presents the first fully kinetic particle-in-cell simulations of partially ionized reconnection and demonstrates that fast reconnection can occur in partially ionized systems. In the simulations, the transition to fast reconnection occurs when the current sheet width thins below the ion-inertial length in contrast to previous analytic predictions. The peak reconnection rate is ≥ 0.08 when normalized to the bulk Alfvén speed (including both ion and neutral mass), consistent with previous experimental results. However, when the bulk Alfvén speed falls below the neutral sound speed, the rate becomes system size dependent. The normalized inflow velocity is ionization fraction dependent, which is shown to be a result of neutral momentum transport. A model for the inflow is developed which agrees well with the simulation results.

DOI: [10.1103/PhysRevLett.122.015101](https://doi.org/10.1103/PhysRevLett.122.015101)

Magnetic reconnection is a ubiquitous process occurring in nearly all magnetized plasmas, during which the global magnetic field topology changes, transferring magnetic energy to plasma particles [1]. Because of the rapid release of stored energy, reconnection has been invoked to explain energetic events observed in natural and laboratory plasmas, and has motivated decades of active research. The majority of this work has focused on hot, fully ionized plasmas, as found in Earth's magnetosphere or the solar corona, yet many space and astrophysical environments are only partially ionized.

For example, the solar chromosphere is relatively cool, dense, and weakly ionized, but contains many classes of dynamical events thought to be driven by reconnection, such as UV bursts [2,3], jets [4,5], spicules [6,7], or transition region explosive events [8]. The importance of partially ionized reconnection to chromospheric physics has motivated several studies of partially ionized reconnection [9–20]. However, a major open question is under what conditions fast (i.e., Alfvénic and resistivity independent) reconnection can occur.

Analytic estimates have predicted a transition to fast, ionization fraction [$\chi \equiv n_i/(n_i + n_n)$] independent reconnection when the current sheet thins below the hybrid inertial length, $d_i\chi^{-1/2}$ where $d_i \equiv c/\omega_{pi}$ is the ion inertial length [13]. Heuristically, this is derived by assuming ions and neutrals are perfectly coupled, replacing the physical ion mass with the effective ion mass, $m_i \rightarrow m_i/\chi$, and scaling results from the fully ionized case (e.g., Birn *et al.* [21]).

These predictions have been tested with mixed results. Experiments report Alfvénic, χ -dependent reconnection [15], while in the absence of plasmoids, fluid simulations report slow reconnection and have concluded that the Hall effect does not significantly modify the reconnection rate [18,19]. To reconcile these results, it was suggested that present reconnection experiments are too small to observe the scale expansion, $d_i \rightarrow d_i\chi^{-1/2}$ [15], but no theory has been developed to explain fluid simulations [19].

In this Letter, we perform the first fully kinetic particle-in-cell simulations of partially ionized reconnection and demonstrate that fast reconnection can occur. Unlike fluid models, kinetic simulations provide a first-principles treatment of dissipation and transport physics (e.g., resistivity, viscosity, heat flux) valid across both collisional and collisionless regimes. Here, only the semicollisionless regime, where the ion-neutral mean free path for momentum exchange λ_{in} is comparable to d_i and electrons are weakly collisional, $\nu_{ei} \ll \Omega_e$, is studied. Electron-neutral collisions are neglected as the Coulomb collision rate, ν_{ei} , is significantly faster than any electron-neutral collision rate. This regime is compatible with both laboratory experiments [15] and the upper solar chromosphere [22]. In these simulations, the transition to fast reconnection occurs when the current sheet thins below d_i . For large neutral beta (ratio of neutral to magnetic field pressures, $\beta_n = 8\pi P_n/B^2$) the global reconnection rate is system size dependent, but is ≥ 0.08 when normalized by the bulk Alfvén speed. The inflow velocity is χ dependent due to

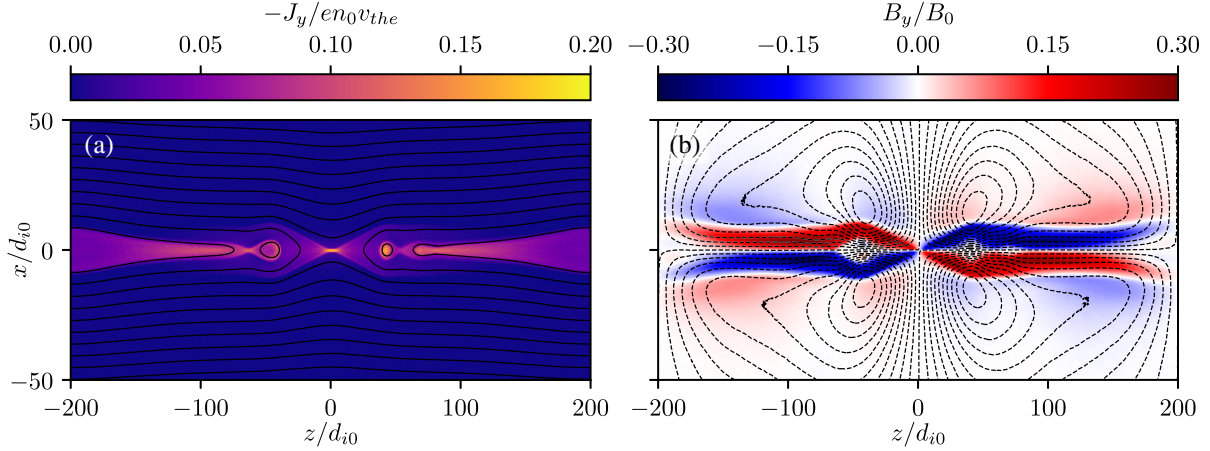


FIG. 1. Example of a partially ionized reconnection simulation from series D with $\chi_0 = 0.1$ showing the central region at time $t\Omega_{i0} = 300$. (a) The out-of-plane current density is shown in color and solid lines are magnetic flux surfaces, (b) the out-of-plane magnetic field in color along with contours of the compressible neutral stream-function (dashed lines). For this case, simulation parameters map to the dimensional parameters $n_e = 1.5 \times 10^{12} \text{ cm}^{-3}$, $B = 28 \text{ G}$ and $L_z = 400d_{i0} = 82 \text{ m}$.

neutral viscous momentum transport, for which a semi-empirical model is developed.

Here we use the explicit, electromagnetic particle-in-cell code VPIC [23]. Coulomb collisions are included using the Takizuka-Abe model [24,25]. Neutrals are evolved kinetically and collisional interactions are included using a Monte Carlo collision model [26] described in the Supplemental Material [27]. The energy-dependent differential cross sections used are based on helium atoms and accurately reproduce measured transport parameters [28,33]. Only elastic collisions are modeled, as inelastic processes (e.g., radiation, ionization, recombination) are estimated to be unimportant for the parameters studied.

The initial setup is an antiparallel Harris sheet with a uniform neutral background. The initial magnetic field, plasma, and neutral density are given by $B_z = B_0 \tanh(x/\delta)$, $n_e = n_i = n_b + n_0 \text{sech}^2(x/\delta)$, and $n_n = n_b(1 - \chi_0)/\chi_0$. This is not an exact equilibrium but relaxes over a few collision times. All species start with the same initial temperature T_0 and the background plasma density is $n_b = 0.3n_0$ corresponding to an upstream $\beta \equiv 8\pi n_e(T_e + T_i)/B^2 = 0.3$. Cross sections are scaled so $T_0 \sim 2 \text{ eV}$, but the only process sensitive to absolute temperature is the neutral viscosity, $\nu_s \approx 0.75v_{A0}d_{i0}$. To seed reconnection, a long-wavelength perturbation is imposed with $A_y = \delta B(L_z/2\pi) \cos(\pi x/L_x) \cos(2\pi z/L_z)$ and $\delta B = 0.0025B_0$. An example case is shown in Fig. 1 and demonstrates the X-line topology and Hall quadrupolar fields typically associated with fast reconnection.

Numerical and physical parameters are listed in Table I. Neutral macroparticles have a larger statistical weight than plasma particles, $w_i = w_e = w_n \chi_0 / (1 - \chi_0)$ and the collision algorithms are applied every five time steps ($0.7\Omega_e^{-1}$). The use of unequal weights has been checked against equal weights at $\chi_0 = 0.1$ with negligible difference.

The collisional-collisionless transition has been predicted to occur when the current sheet thins below the hybrid inertial scale, $d_i \chi^{1/2}$ [13]; however previous two-fluid simulations have not seen this transition [18,19]. To test this, we follow the approach of Daughton *et al.* [24] and simulations with current sheets initially thicker than $d_i \chi^{1/2}$ are performed.

The global reconnection rate is computed as $R = cE_y/Bv_A$ where E_y is evaluated at the X point and Bv_A is evaluated $25d_{i0}$ upstream. In this Letter, $v_A = B/(4\pi m_i n_i)^{1/2}$ is the ion Alfvén speed and does not include neutral density. Figure 2(a) shows this rate weighted by $\chi^{-1/4}$ as measured at the X point, a factor predicted by Malyshkin and Zweibel [13] for the resistive (Sweet-Parker) regime. In this limit, the change $m_i \rightarrow m_i/\chi$ leads to a reduced Alfvén velocity and Lundquist number. Carrying out the Sweet-Parker analysis yields $R \approx S^{-1/2} \chi^{1/4}$. Early in time, all cases undergo collisional reconnection and this scaling holds, as evidenced by $R\chi^{-1/4}$ invariant across cases.

TABLE I. Simulation parameters. All cases have $m_i/m_e = 40$, $\omega_{pe}/\Omega_e = 2$, $c/v_{the} = 4$, $\nu_{ei}^{\text{mom}}/\Omega_e = \sqrt{m_e/m_i} \nu_{ii}^{\text{mom}}/\Omega_i = 0.02$, $\nu_{in}^{\text{mom}}/\Omega_i = 1$, and $\nu_{nn}^{\text{visc}}/\Omega_i = 0.25$ corresponding to the mean free paths $\lambda_{ei}^{\text{mom}}/d_i = \lambda_{ii}^{\text{mom}}/d_i = 4$, $\lambda_{in}^{\text{mom}}/d_i = 0.5$, and $\lambda_{nn}^{\text{visc}}/d_i = 2$. For each series, multiple cases are performed with varying χ ($0.01 < \chi_0 \leq 1$).

Series	δ_0/d_i	L_x/d_i	L_z/d_i	n_x	n_z	Particles
A	2.5	50	100	790	1560	1.0×10^9
B	1	50	100	790	1560	3.5×10^9
C	1	100	200	1580	3040	1.5×10^9
D	1	200	400	3162	6240	1.7×10^{10}

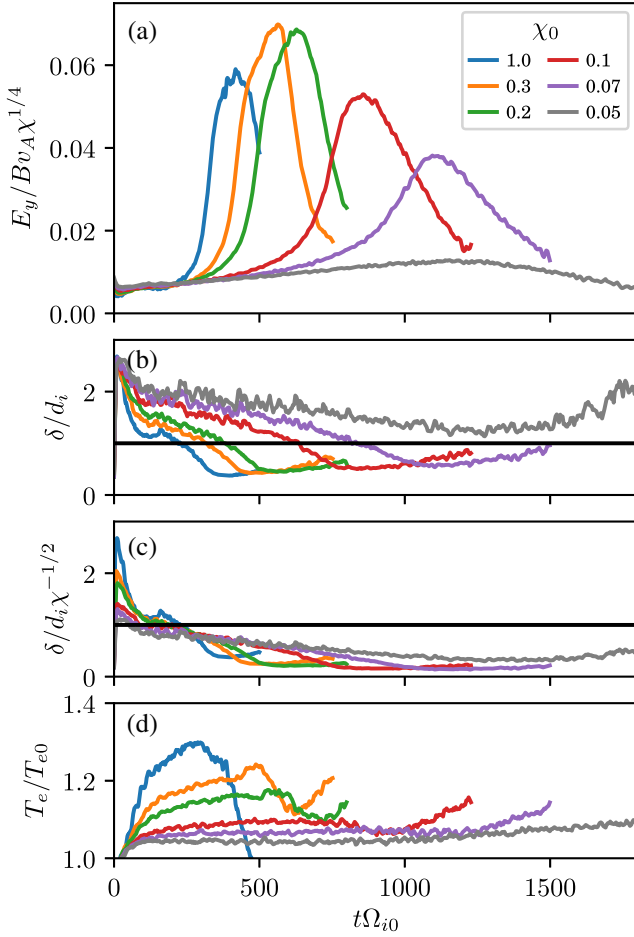


FIG. 2. Transition between collisional and collisionless reconnection in series A. Panels show (a) the scaled reconnection rate, (b) and (c) the minimum current sheet width normalized to the local ion inertial length d_i and the hybrid inertial length $d_i \chi^{-1/2}$, and (d) the electron temperature at the X point.

All except the $\chi_0 = 0.05$ case transition to fast reconnection later in time, although the peak rate in the collisionless regime is χ dependent. To test the transition criteria, the local current sheet thickness δ is measured and normalized to both d_i and $d_i \chi^{-1/2}$, Figs. 2(b) and 2(c). In all cases, the current sheet thins below $d_i \chi^{-1/2}$; however the transition in reconnection rate is more closely correlated with the condition $\delta / d_i \approx 1$. Supporting this, the case $\chi_0 = 0.05$ does not transition despite satisfying $d_i \chi^{-1/2} > \delta \gtrsim d_i$.

The failure to transition can be understood by examining the electron temperature at the X line, Fig. 2(d). On reconnection timescales, all species are well coupled, but for decreasing χ , the larger neutral fraction increases the total heat capacity, thereby reducing the temperature rise at the X line. As a result, in the $\chi_0 = 0.05$ case, T_e and η remain nearly constant over time. This reduced temperature rise prevents Ohmic heating from thinning the current sheet below d_i as was seen in previous fully ionized simulations [34]. This suggests that while transport physics are

important in understanding the detailed behavior of the collisional-collisionless transition at moderate to high ionization fractions, for low χ , isothermal models [35,36] are more appropriate.

To examine the dependence of the reconnection rate, simulations were performed with a thinner initial current sheet width of $1d_{i0}$ such that all cases transition to fast reconnection. Here we distinguish between the global rate, as defined above, and the local reconnection rate defined by u_{in}/v_A where u_{in} is the peak inflow speed in the center of mass frame. These measures are plotted at the time of peak global reconnection rate in Fig. 4.

For $\chi \gtrsim 0.15$ the global rate scales with the bulk Alfvén speed as $R = 0.08\chi^{1/2}$, equivalent to a constant, fast rate of 0.08 if the definition of v_A included neutrals. In this study, $\beta_i = 0.3$ is held fixed, and the neutral beta is $\beta_n = \beta_i/\chi$. For $\chi \leq 0.15$, $\beta_n \geq 2$ and the bulk Alfvén speed falls below the neutral sound speed. In this regime, R becomes χ independent, and for $L_z = 100d_{i0}$ follows the scaling $R = 0.075v_{\text{MS}}/v_A$ where v_{MS} is the coupled magnetosonic phase speed $v_{\text{MS}}/v_A = (\chi + \beta_i/2)^{1/2}$ [37]. In larger systems, the rate is reduced suggesting that in very large systems the rate may continue to scale with the bulk Alfvén speed. The detailed physics underlying the χ and system size dependence in this regime are not yet fully understood and will be explored in a future manuscript.

The local rate does not depend on system size and scales as $u_{\text{in}}/v_A \sim \chi^{1.2}$. This differs from, but is related to, the global rate, and in a well-coupled, steady-state system they should be equivalent. This is typically the case for fully ionized systems; however in partially ionized systems decoupling of ion and neutral flows can break this relationship [9,14]. Flow decoupling, while present, is not sufficient to explain these results. Rather, at the time of peak rate the maximum u_{in} occurs at the edge of the ion diffusion region and there is a transient, non-uniform \mathbf{E} . As a result, the local $\mathbf{E} \times \mathbf{B}$ velocity differs from the global E_y/B and thus u_{in}/v_A differs from R .

Locally, the electric field is supported at the X line by the nongyrotropic electron pressure tensor [38], Fig. 3, $E_{\text{NG}} \equiv -(\nabla \cdot \mathbf{P}_e)_y / en$. For E_{NG} to be significant, δ must be on the order of the electron gyroradius, ρ_e , and in all cases $\delta/\rho_e \approx 0.3-0.5$, where ρ_e is evaluated at 1δ upstream of the X line. Furthermore, as a consequence of momentum conservation and the collisional couplings, neutral viscosity must also be included. The momentum equations are

$$m_e n_e \frac{d\mathbf{v}_e}{dt} = -en_e \left(\mathbf{E} + \frac{\mathbf{v}_e \times \mathbf{B}}{c} \right) - \nabla \cdot \mathbf{P}_e - \mathbf{R}_{ie} \quad (1a)$$

$$m_i n_i \frac{d\mathbf{v}_i}{dt} = en_i \left(\mathbf{E} + \frac{\mathbf{v}_i \times \mathbf{B}}{c} \right) - \nabla \cdot \mathbf{P}_i + \mathbf{R}_{ie} + \mathbf{R}_{in} \quad (1b)$$

$$m_n n_n \frac{d\mathbf{v}_n}{dt} = -\nabla \cdot \mathbf{P}_n - \mathbf{R}_{in}, \quad (1c)$$

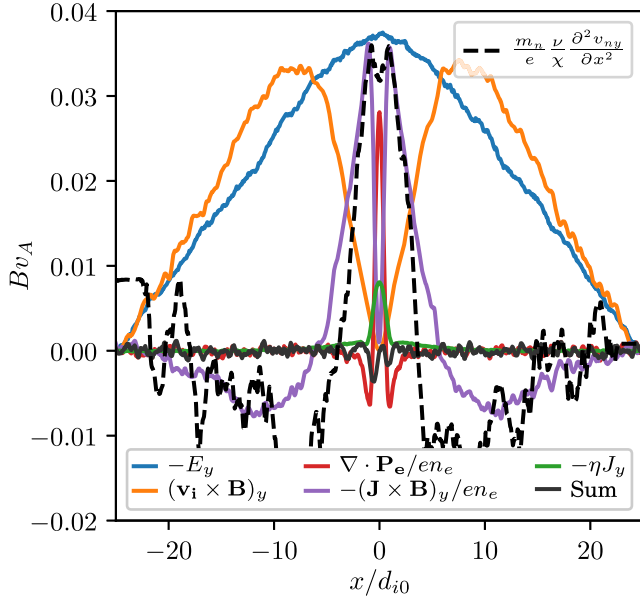


FIG. 3. Evaluation of the terms in Ohm's law along the inflow of the $\chi_0 = 0.1$ case from series B at $t\Omega_{i0} = 175$. The ion diffusion region is defined by $\mathbf{J} \times \mathbf{B} < 0$ corresponding to $|x| < 6.5d_{i0}$. Equation (3) is tested by plotting the right-hand side as the dashed line. To reduce noise, $\partial^2 v_{ny}/\partial x^2$ is averaged over $\pm 2.5d_{i0}$.

where $\mathbf{R}_{ab} = -\mathbf{R}_{ba}$ is the frictional force on species a from species b . In steady state and at the X line, $\mathbf{B} = 0$ and $\mathbf{v}_s = v_{s,y}\hat{\mathbf{y}}$ due to symmetry. Using this and adding the y components, the constraint

$$en_e E_{\text{NG}} = [\nabla \cdot (\mathbf{P}_i + \mathbf{P}_n)]_y \quad (2)$$

is obtained.

When ions and neutrals are the same atomic species, the dominant collisional process is symmetric charge exchange, and collision integrals can be evaluated [39]. In the limit $\nu_{\text{in}} \gtrsim \Omega_i \gg |\nabla \mathbf{v}_i|$ and $v_{th,i} \gg |\mathbf{v}_i - \mathbf{v}_n|$, the pressure tensors are efficiently coupled, and to lowest order $\mathbf{P}_i \approx n_i \mathbf{P}_n / n_n$.

In the weakly ionized limit and on length scales above the neutral mean free path, the neutral pressure tensor can be closed using an incompressible hydrodynamic closure, $\mathbf{P}_n = P_n - m_n n_n \nu_s [\nabla \mathbf{v}_n + (\nabla \mathbf{v}_n)^T]$ where ν_s is the kinematic shear viscosity and P_n the scalar pressure. On shorter length scales, kinetic corrections are present [40,41], but this closure can still be used to roughly estimate the neutral pressure tensor near the X line. Combining these closures with Eq. (2) gives

$$E_{\text{NG}} = -\frac{m_n \nu_s}{e \chi} \nabla^2 v_{n,y} \approx -\frac{m_n \nu_s}{e \chi} \frac{\partial^2 v_{n,y}}{\partial x^2}, \quad (3)$$

which is tested in Fig. 3(a) and approximately holds.

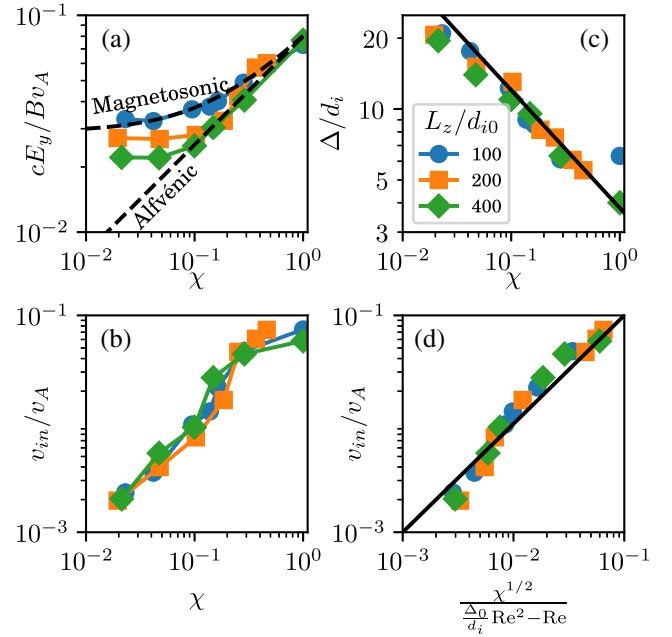


FIG. 4. Ionization fraction and system size dependence of (a) the global reconnection rate, (b) the local inflow velocity, and (c) the ion diffusion region thickness for series B–D. Labeled lines in (a) show the scalings $R = 0.08\chi^{1/2}$ (Alfvénic) and $R = 0.075(\chi + \beta_i/2)^{1/2}$ (Magnetosonic). In (c), the solid line is $\Delta/d_i = 4\chi^{-1/2}$. In panel (d), Eq. (6) is tested using $\Delta_0 = 4d_i$ and $\theta = 1$ with the solid line showing equality.

A result of this out-of-plane flow is that the local inflow is limited by momentum balance within the ion-diffusion region. The total y -momentum deposition rate must be balanced by inward and outward transport,

$$\begin{aligned} \frac{\Delta L}{c} (\mathbf{J} \times \mathbf{B})_y &= m(n_i + n_n)(\Delta u_{z,\text{out}} u_y - L u_{x,\text{in}} u_{y,\text{in}}) \\ &+ \Delta P_{yz,\text{out}} - L P_{xy,\text{in}}, \end{aligned} \quad (4)$$

where Δ and L are the half-width and half-length of the ion-diffusion region, respectively, \mathbf{u} is the center-of-mass velocity, and P_{ab} is the total pressure tensor. For simplicity, we will neglect flow decoupling so $\mathbf{u} = \mathbf{v}_i = \mathbf{v}_n$, approximate the ratio of momentum transport by advection relative to internal stress by $m(n_i + n_n)u_{x,\text{in}}u_{y,\text{in}}/P_{xy,\text{in}} \approx u_{x,\text{in}}\Delta/\nu_s$, and the $(\mathbf{J} \times \mathbf{B})_y$ force by $en_i E_y$. Then, along with Eq. (3), Eq. (4) can be solved for $u_{x,\text{in}}$,

$$u_{x,\text{in}} = \frac{\nu_s}{\Delta} \frac{u_{y,\text{in}}}{u_y - u_{y,\text{in}}}. \quad (5)$$

At the edge of the ion diffusion region $u_{x,\text{in}} = cE_y/B_{z,\text{in}}$ which, using Eq. (3), gives $u_y = u_{x,\text{in}}\Delta^2\chi\Omega_n/\nu_s$, where $\Omega_n \equiv eB_{z,\text{in}}/m_n c$. Inserting this into Eq. (5) allows the inflow velocity to be parametrized as a function of the

inflow velocity angle $\theta \equiv u_{y,\text{in}}/u_{x,\text{in}}$. Empirically we find $\theta \approx 1 \pm 0.2$ ($\tan^{-1}\theta = 40^\circ\text{--}50^\circ$), although we do not have a physical explanation for this. Further simplification is achieved by noting that $\Delta = \Delta_0\chi^{-1/2}$, as shown in Fig. 4(c) and predicted by Malyshkin and Zweibel [13] by making the replacement $d_i \rightarrow d_i\chi^{-1/2}$. Using this and assuming $\theta = 1$ gives the prediction

$$\frac{u_{x,\text{in}}}{v_{A,\text{in}}} = \frac{\chi^{1/2}}{\frac{\Delta_0}{d_i}\text{Re}^2 - \text{Re}}, \quad (6)$$

where $\text{Re} \equiv \Delta_0 v_{A,\text{in}}/\nu_s$ is the characteristic Reynolds number and $v_{A,\text{in}}$ is the Alfvén velocity evaluated using $B_{z,\text{in}}$. This equation is tested in Fig. 4(d) using the value $\Delta_0 = 4d_i$. Good agreement is obtained over all cases despite the simplicity of this model, and can be improved further by using the measured θ (not shown).

Equation (6) determines the local reconnection rate based on the ionization fraction and the magnetic field strength at the edge of the ion diffusion region. Although sufficient to describe the present results, Eq. (6) predicts a vanishing local rate in the limit $\nu_s \rightarrow 0$. In this limit resistive dissipation likely dominates and the assumption $E_y = E_{\text{NG}}$ no longer holds.

This Letter presents the first fully kinetic simulations of partially ionized reconnection and examines the scaling of the reconnection rate and the transition from collisional to collisionless reconnection. Fast reconnection in partially ionized systems is demonstrated for the first time, the transition to which occurs when the current sheet thins below d_i . The global reconnection rate scales with the bulk Alfvén velocity when $\beta_n < 2$, but for $\beta_n > 2$ the rate is system size dependent and appears to scale with magnetosonic speed in small domains. This effect is not yet understood and will be examined further in future work. In the cases studied, the neutral viscosity balances the $\mathbf{J} \times \mathbf{B}$ force, which differs from both ambipolar diffusion (where the inertial force balances $\mathbf{J} \times \mathbf{B}$ [42]) and from inviscid multifluid models [13]. As a result, the inflow velocity is χ dependent due to viscous momentum transport.

This work studies single X lines in preexisting thin current sheets, but understanding how and when such current sheets could form is an important question. Ambipolar diffusion [43], turbulence [44], and plasmoid instability [34,45–48] are known mechanisms for producing thin current sheets, but in the absence of such mechanisms fast reconnection may be inhibited. Although there is currently no comprehensive theory of partially ionized plasmoid instability, previous fluid studies have routinely observed plasmoids [14,16,18], suggesting that it may be a generic and important process in very weakly ionized systems such as the lower solar chromosphere.

Digital data presented in this manuscript can be accessed in the Princeton University DataSpace [49].

The authors gratefully acknowledge funding from both the Basic Plasma Science Program from DOE Office of Fusion Energy Sciences under Contract No. DE-AC02-09CH11466 and from NASA under Grant No. NNH15AB29I. The simulations presented in this article were performed on computational resources managed and supported by Princeton Research Computing, a consortium of groups including the Princeton Institute for Computational Science and Engineering (PICSciE) and the Office of Information Technology’s High Performance Computing Center and Visualization Laboratory at Princeton University.

-
- [1] M. Yamada, R. Kulsrud, and H. Ji, *Rev. Mod. Phys.* **82**, 603 (2010).
 - [2] F. Ellerman, *Astrophys. J.* **46**, 298 (1917).
 - [3] H. Peter *et al.*, *Science* **346**, 1255726 (2014).
 - [4] D. Innes, B. Inhester, W. Axford, and K. Wilhelm, *Nature (London)* **386**, 811 (1997).
 - [5] K. Shibata *et al.*, *Science* **318**, 1591 (2007).
 - [6] B. De Pontieu, S. McIntosh, V. H. Hansteen, M. Carlsson, C. J. Schrijver, T. D. Tarbell, A. M. Title, R. A. Shine, Y. Suematsu, S. Tsuneta, Y. Katsukawa, K. Ichimoto, T. Shimizu, and S. Nagata, *Publ. Astron. Soc. Jpn.* **59**, S655 (2007).
 - [7] L. Hegglund, B. De Pontieu, and V. Hansteen, *Astrophys. J.* **702**, 1 (2009).
 - [8] P. Chen and E. Priest, *Sol. Phys.* **238**, 313 (2006).
 - [9] E. G. Zweibel, *Astrophys. J.* **340**, 550 (1989).
 - [10] J. I. Sakai, K. Tsuchimoto, and I. V. Sokolov, *Astrophys. J.* **642**, 1236 (2006).
 - [11] J. I. Sakai and P. D. Smith, *Astrophys. J. Lett.* **687**, L127 (2008).
 - [12] J. I. Sakai and P. D. Smith, *Astrophys. J. Lett.* **691**, L45 (2009).
 - [13] L. M. Malyshkin and E. G. Zweibel, *Astrophys. J.* **739**, 72 (2011).
 - [14] J. E. Leake, V. S. Lukin, M. G. Linton, and E. T. Meier, *Astrophys. J.* **760**, 109 (2012).
 - [15] E. E. Lawrence, H. Ji, M. Yamada, and J. Yoo, *Phys. Rev. Lett.* **110**, 015001 (2013).
 - [16] J. E. Leake, V. S. Lukin, and M. G. Linton, *Phys. Plasmas* **20**, 061202 (2013).
 - [17] L. Ni, B. Kliem, J. Lin, and N. Wu, *Astrophys. J.* **799**, 79 (2015).
 - [18] N. A. Murphy and V. S. Lukin, *Astrophys. J.* **805**, 134 (2015).
 - [19] L. Ni, V. S. Lukin, N. A. Murphy, and J. Lin, *Astrophys. J.* **852**, 95 (2018).
 - [20] L. Ni, V. S. Lukin, N. A. Murphy, and J. Lin, *Phys. Plasmas* **25**, 042903 (2018).
 - [21] J. Birn, J. F. Drake, M. A. Shay, B. N. Rogers, R. E. Denton, M. Hesse, M. Kuznetsova, Z. W. Ma, A. Bhattacharjee, A. Otto, and P. L. Pritchett, *J. Geophys. Res. Space Phys.* **106**, 3715 (2001).

- [22] E. H. Avrett and R. Loeser, *Astrophys. J. Suppl. Ser.* **175**, 229 (2008).
- [23] K. J. Bowers, B. J. Albright, L. Yin, B. Bergen, and T. J. T. Kwan, *Phys. Plasmas* **15**, 055703 (2008).
- [24] W. Daughton, V. Roytershteyn, B. Albright, H. Karimabadi, L. Yin, and K. J. Bowers, *Phys. Plasmas* **16**, 072117 (2009).
- [25] T. Takizuka and H. Abe, *J. Comput. Phys.* **25**, 205 (1977).
- [26] C. K. Birdsall, *IEEE Trans. Plasma Sci.* **19**, 65 (1991).
- [27] See Supplemental Material at <http://link.aps.org/supplemental/10.1103/PhysRevLett.122.015101> for a description of the collision algorithm and benchmarks, along with Refs. [28–32].
- [28] H. Wang, V. S. Sukhomlinov, I. D. Kaganovich, and A. S. Mustafaev, *Plasma Sources Sci. Technol.* **26**, 024001 (2017).
- [29] H. Helm, *J. Phys. B* **9**, 1171 (1976).
- [30] H. Petersen, The properties of helium: Density, specific heats, viscosity, and thermal conductivity at pressures from 1 to 100 bar and from room temperature to about 1800 K, Danish Atomic Energy Commission, Risoe Research Establishment Technical Report No. 224, 1970.
- [31] A. Phelps, C. H. Greene, and J. Burke, Jr., *J. Phys. B* **33**, 2965 (2000).
- [32] A. Phelps, Helium-helium elastic scattering, http://jila.colorado.edu/avp/collision_data/neutralneutral/atomatom.txt.
- [33] L. Xu, A. V. Khrabrov, I. D. Kaganovich, and T. J. Sommerer, *Phys. Plasmas* **24**, 093511 (2017).
- [34] W. Daughton, V. Roytershteyn, B. J. Albright, H. Karimabadi, L. Yin, and K. J. Bowers, *Phys. Plasmas* **16**, 072117 (2009).
- [35] P. A. Cassak, J. F. Drake, M. A. Shay, and B. Eckhardt, *Phys. Rev. Lett.* **98**, 215001 (2007).
- [36] P. A. Cassak, M. A. Shay, and J. F. Drake, *Phys. Plasmas* **17**, 062105 (2010).
- [37] T. C. Mouschovias, G. E. Ciolek, and S. A. Morton, *Mon. Not. R. Astron. Soc.* **415**, 1751 (2011).
- [38] M. Hesse, K. Schindler, J. Birn, and M. Kuznetsova, *Phys. Plasmas* **6**, 1781 (1999).
- [39] R. Schunk, *Rev. Geophys.* **15**, 429 (1977).
- [40] S. Chapman, T. G. Cowling, and D. Burnett, *The Mathematical Theory of Non-Uniform Gases: An Account of the Kinetic Theory of Viscosity, Thermal Conduction and Diffusion in Gases* (Cambridge University Press, Cambridge, England, 1970).
- [41] L. Woods, *J. Fluid Mech.* **136**, 423 (1983).
- [42] J. Leake, C. DeVore, J. Thayer, A. Burns, G. Crowley, H. Gilbert, J. Huba, J. Krall, M. Linton, V. Lukin *et al.*, *Space Sci. Rev.* **184**, 107 (2014).
- [43] A. Brandenburg and E. G. Zweibel, *Astrophys. J.* **427**, L91 (1994).
- [44] A. Rappazzo and E. Parker, *Astrophys. J. Lett.* **773**, L2 (2013).
- [45] N. F. Loureiro, A. A. Schekochihin, and S. C. Cowley, *Phys. Plasmas* **14**, 100703 (2007).
- [46] A. Bhattacharjee, Y.-M. Huang, H. Yang, and B. Rogers, *Phys. Plasmas* **16**, 112102 (2009).
- [47] Y.-M. Huang and A. Bhattacharjee, *Phys. Plasmas* **17**, 062104 (2010).
- [48] H. Ji and W. Daughton, *Phys. Plasmas* **18**, 111207 (2011).
- [49] See <https://dataspace.princeton.edu/jspui/handle/88435/dsp01x920g025r>.